

Thermostating highly confined fluids

Stefano Bernardi,^{1,a)} B. D. Todd,^{1,b)} and Debra J. Searles^{2,c)}

¹Centre for Molecular Simulation, Swinburne University of Technology, Hawthorn, Victoria 3122, Australia

²Queensland Micro- and Nanotechnology Centre, School of Biomolecular and Physical Sciences, Griffith University, Brisbane, Queensland 4111, Australia

(Received 23 April 2010; accepted 20 May 2010; published online 29 June 2010)

In this work we show how different use of thermostating devices and modeling of walls influence the mechanical and dynamical properties of confined nanofluids. We consider a two dimensional fluid undergoing Couette flow using nonequilibrium molecular dynamics simulations. Because the system is highly inhomogeneous, the density shows strong fluctuations across the channel. We compare the dynamics produced by applying a thermostating device directly to the fluid with that obtained when the wall is thermostated, considering also the effects of using rigid walls. This comparison involves an analysis of the chaoticity of the fluid and evaluation of mechanical properties across the channel. We look at two thermostating devices with either rigid or vibrating atomic walls and compare them with a system only thermostated by conduction through vibrating atomic walls. Sensitive changes are observed in the xy component of the pressure tensor, streaming velocity, and density across the pore and the Lyapunov localization of the fluid. We also find that the fluid slip can be significantly reduced by rigid walls. Our results suggest caution in interpreting the results of systems in which fluid atoms are thermostated and/or wall atoms are constrained to be rigid, such as, for example, water inside carbon nanotubes. © 2010 American Institute of Physics. [doi:10.1063/1.3450302]

I. INTRODUCTION

Nonequilibrium molecular dynamics (NEMD) has seen a significant growth in recent years because of the possibility of studying transport coefficients and rheological properties of fluids out of equilibrium, thus mimicking real experiments.¹ Two classes of algorithms can be distinguished, homogeneous² and inhomogeneous.³ The former class makes use of appropriate periodic boundary conditions (PBCs) in all directions to simulate a bulk region of fluid, avoiding problematic surface effects close to the boundaries. The external forces are implemented directly into the equations of motion to generate the flux of interest and the corresponding transport coefficients can be directly determined.⁴ In inhomogeneous methods, wall boundaries constrain the fluid in a defined geometry and the system is driven away from equilibrium by the movement of the walls themselves, as in the case of Couette flow, or by the use of an external force field, a pressure gradient or a gravitylike force, as in the case of Poiseuille flow. In both methods, however, work is performed on the fluid, and viscous heating has to be extracted in order to reach a steady state. In homogeneous methods a thermostat is applied directly to the fluid particles, while in inhomogeneous methods the thermostat is usually applied either on the wall particles exclusively or fluid and wall particles together or only fluid particles, depending on how the wall is implemented in the simulations.

The use of homogeneous algorithms has been rapidly increasing, particularly for molecular fluids such as poly-

mers, where the systems' dimension is critical, and due to the possibility of reproducing complex types of flow (e.g., elongation) indefinitely.² Also if the underlying equations of motion are SLLOD, a link with nonlinear response theory is possible.⁴ However, due to an increasing interest in nanoconfined systems, more effort has been invested in modeling systems with walls.

In intensive computations carried out in nanopores, as in the case of flows of water in carbon nanotubes or molecules in porous media, where the channel diameter can be of the order of a few nanometers, uniform thermostats are often applied to the fluid. The walls can either be modeled by "frozen" particles, fixed in their equilibrium positions,^{5,6} or by vibrating particles.^{7,8} In nanopores the fluctuations in density become important, making the use of simple uniform thermostats inappropriate. Depending on the purpose of the simulation, this may not be a primary concern, and the influence on the results negligible. However, in other situations in which precise measurements are being attempted, the results could be significantly affected by inappropriate thermostating.

The definition of temperature for nonequilibrium systems is still an open problem.⁹ The thermodynamic expression for the temperature is in fact linked to the definition of the entropy, which, for nonequilibrium steady states, is still under debate.^{10,11} However, it is commonly accepted that the majority of the systems under study satisfy the *local thermodynamic equilibrium postulate*.¹² This is true if the inhomogeneities both in space and time are small enough to be ignored on a microscopic scale. The kinetic temperature, a common choice in NEMD, is defined as

^{a)}Electronic mail: sbernardi@ict.swin.edu.au.

^{b)}Electronic mail: btodd@swin.edu.au.

^{c)}Electronic mail: d.bernhardt@griffith.edu.au.

$$T_K(t) = \frac{\sum_i m_i [\mathbf{v}_i(t) - \mathbf{u}(\mathbf{r}_i, t)]^2}{dNk_B}, \quad (1)$$

where N is the number of particles, d the Cartesian dimension, k_B the Boltzmann constant, m_i the mass per particle, \mathbf{r}_i and \mathbf{v}_i are the position and laboratory velocity, respectively, of particle i , and $\mathbf{u}(\mathbf{r}_i, t)$ the instantaneous streaming velocity. This is assumed to be the same as the entropic temperature

$$\frac{1}{T_s} = \left. \frac{\partial S}{\partial E} \right|_V. \quad (2)$$

This is in general not true, but the kinetic temperature is a good operational choice. The determination of the streaming velocity is, however, a delicate point because its incorrect evaluation could cause a thermostat, which makes use of this definition, to induce an unphysical behavior on the particles. An example is the production of a string phase for homogeneous Couette flow.¹³ For inhomogeneous systems, because of the strong density fluctuations in space, the local thermodynamic equilibrium postulate is valid only if considering slices of the simulation cell in which the variation in density is negligible (however, for very high external fields this assumption is no longer true). Thus, a proper thermostat that is applied to the fluid will have to account for this inhomogeneity. The most common are the Gaussian isokinetic¹ and Nosé–Hoover¹⁴ thermostats. Both have the characteristic of being deterministic and time reversible, both facilitating analysis by dynamical systems theory. We will use the Nosé–Hoover thermostat because it is also able to reproduce the canonical distribution function at equilibrium.¹⁴

Our analysis will extend to mechanical and dynamical properties for a fluid undergoing planar Couette flow (PCF). Although we restrict our research to this flow geometry, our conclusions can be extended to other flows, such as Poiseuille flow, where a confinement is also present. We will consider pressure, temperature, and density profiles across the channel, speed and velocity distributions, and the Lyapunov spectra and Lyapunov localization of the fluid to analyze the chaotic properties. The Lyapunov spectra, which are the ordered collection of Lyapunov exponents, describe what happens to the trajectories in the phase space, giving knowledge of the particle dynamics and their chaotic behavior. The Lyapunov exponents describe the mean exponential rate of growth or convergence of neighboring trajectories in phase space.¹⁵ The Lyapunov exponents have been computed extensively for bulk systems subjected to different types of flow,^{16–22} and in a previous paper we showed the spectra of the whole phase space for an inhomogeneous fluid.²³ In this work we are however interested only in the fluid phase space. To better compare the dynamics in the phase space we also show the Lyapunov spectra for a homogeneous fluid evolving according to the SLLOD equations of motion at the same state point as that of the inhomogeneous fluid. A recent discussion regarding the differences in stresses between the homogeneous SLLOD shear algorithm and the boundary driven case can be found in Refs. 24 and 25. We will not discuss the details concerning the method employed to com-

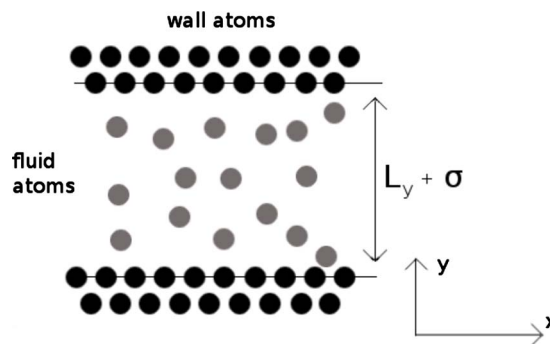


FIG. 1. Schematic representation of the simulation box.

pute the Lyapunov exponents, the algorithm of Benettin *et al.*,^{26,27} but refer readers to these original papers or our previous paper.²³

II. METHODOLOGY

In this work we have used a two dimensional atomic fluid flowing in a channel of a few atomic diameters σ . The channel is periodic in the x direction and the walls are composed of particles (Fig. 1). The particles (both fluid and walls) interact with each other by a smooth repulsive potential, the Weeks–Chandler–Anderson (WCA) potential,²⁸ which neglects the attractive component of the interatomic force

$$\Phi_{\text{WCA}} = \begin{cases} 4\epsilon \left[\left(\frac{\sigma}{q_{ij}} \right)^{12} - \left(\frac{\sigma}{q_{ij}} \right)^6 \right] + \epsilon, & q_{ij} \leq 2^{1/6}\sigma \\ 0, & q_{ij} > 2^{1/6}\sigma, \end{cases} \quad (3)$$

where $q_{ij} = |\mathbf{q}_i - \mathbf{q}_j|$ with \mathbf{q}_i being the laboratory particle position, σ and ϵ are the interaction range and the energy parameters, respectively. All the physical units are expressed in reduced units where the unit of mass is the particle mass m , the energy unit is the parameter ϵ , and the length unit is σ .²⁹ Furthermore, we define $m = \sigma = \epsilon = k_B = 1$.

For the wall, two cases are presented: the first in which a harmonic potential tethers each particle to a virtual lattice site leaving it free to vibrate around its equilibrium position; and the second in which the particles are frozen. Frozen wall particles have no peculiar momentum. The harmonic potential is

$$\Phi_H(|\mathbf{q}^W - \mathbf{q}^L|) = \frac{1}{2}k_w |\mathbf{q}^W - \mathbf{q}^L|^2, \quad (4)$$

where the superscripts W and L indicate the wall particle and its lattice site, respectively, and the spring constant k_w has been set to 150, a common value in the literature (e.g., see Ref. 30). Couette flow is induced by shifting the position of the wall particles or their virtual lattice sites at each time step along the x direction such that

$$\Delta q_x^l = \pm \frac{1}{2} \dot{\gamma} L_y \Delta t, \quad (5)$$

where q_x^l is the x coordinate of the lattice site, $L_y + \sigma$ is the distance between the two walls, as defined in Fig. 1, and Δt is the time step.

The system is composed of 45 fluid particles and 40 wall particles, 20 for each wall organized in two layers of ten

atoms each. The wall particle density has been set to $\rho_w = 0.8$ and the fluid at $\rho_f = 0.6$. The channel is $L_y = 6.82$ wide and $L_x = 11.18$ in length. The number of particles is small because the computation of the Lyapunov spectra is computationally intensive. However, we stress that the purpose of the present paper is not to provide meaningful rheological results to compare with real experiments, but rather to show the effects related to the use of different thermostating devices. The mechanical properties in the case of the wall-only thermostated (WT) system have been computed for a system with 250 fluid particles and no significant changes in the off-diagonal pressure, density, temperature, and streaming velocity profiles have been detected (see also, for example, Ref. 30).

III. THERMOSTATING DEVICES AND EQUATIONS OF MOTION

The thermostating devices presented here are the profile biased thermostat (PBT) and profile unbiased thermostat (PUT).⁴ A PBT is a thermostat that makes assumptions on the streaming velocity of particles. The problem regarding its use was first explored by Evans and Morriss¹³ to explain the formation of the so-called string phase for homogeneous shear systems observed by Erpenbeck³¹ in 1984. It is particularly common in modeling PCF to assume that the streaming velocity profile is linear. This is, however, not always the case, especially for high strain rates and high Reynolds numbers or for very highly confined fluids. If the streaming velocity differs from the expected values the thermostat will interpret this difference as if the system were heating up, suppressing the formation of secondary flows. For boundary driven Couette flow the streaming velocity at the boundary will not be linear and therefore a PUT should always be the preferred choice. For the PBT we consider the case in which the fluid is treated as homogeneous. The PUT does not need this distinction, in fact the variation in density is automatically accounted for during the instantaneous evaluation of the streaming velocity. For both PBT and PUT with a vibrating wall, the Nosé–Hoover thermostat has been applied also to the wall to avoid the fluid acting as a thermal reservoir for the wall particles.

The equations of motion for the wall particles connected to the virtual lattice by a Hookean potential are

$$\dot{\mathbf{q}}_i^w = \mathbf{p}_i^w/m_i^w, \quad (6)$$

$$\dot{\mathbf{p}}_i^w = \mathbf{F}_i^w - \xi^w \mathbf{p}_i^w, \quad (7)$$

$$\dot{\xi}^w = \frac{1}{Q} \left[\sum_i \frac{\mathbf{p}_i^{w2}}{m_i^w} - g N_w k_B T \right], \quad (8)$$

where g represents the Cartesian degrees of freedom (2 in this case), and the superscript w identifies wall particles. \mathbf{F}_i^w includes the term due to the spring potential.

When the wall atoms are frozen there are no equations of motion and their position changes according to Eq. (5), where this time q_x^l has to be substituted with the real particle coordinates. The fluid particles for the wall thermostated system move according to Newton's equations of motion,

$$\dot{\mathbf{q}}_i^f = \mathbf{p}_i^f/m_i^f, \quad (9)$$

$$\dot{\mathbf{p}}_i^f = \mathbf{F}_i^f, \quad (10)$$

while if the fluid is thermostated,

$$\dot{\mathbf{q}}_i^f = \mathbf{p}_i^f/m_i^f, \quad (11)$$

$$\dot{\mathbf{p}}_i^f = \mathbf{F}_i^f - \xi^f \mathbf{p}_i^f, \quad (12)$$

where the friction coefficient ξ^f and the term \mathbf{p}_i^f take different forms depending on the thermostat device type (PUT, PBT). The differences depend on the definition of the streaming velocity in the x direction to obtain the peculiar velocity. For the PBT thermostat the velocity gradient is assumed to vary linearly across the channel,

$$v_x(y) = \dot{\gamma}y, \quad (13)$$

where $\dot{\gamma}$ is the shear strain rate. This assumption is good for low shear rate and homogeneous fluids (as in the SLLOD algorithm); however, for highly confined systems it is not valid anymore, at least in the region close to the wall.

We now introduce the microscopic density and the momentum density used for computation of the streaming velocity and the temperature at a chosen position in the system. The mass density in the position \mathbf{r} and time t is defined as

$$\rho(\mathbf{r}, t) = \sum_i m_i \delta(\mathbf{r} - \mathbf{r}_i(t)), \quad (14)$$

and the momentum density as

$$\mathbf{J}(\mathbf{r}, t) = \rho(\mathbf{r}, t) \mathbf{u}(\mathbf{r}, t) = \sum_i m_i \mathbf{v}_i(t) \delta(\mathbf{r} - \mathbf{r}_i(t)), \quad (15)$$

where $\mathbf{u}(\mathbf{r}, t)$ is the streaming velocity and $\delta(\mathbf{r})$ is the Dirac delta function. In a simulation, the channel is divided into slabs (or bins) of finite size, $\Delta = 0.05$, aligned with the wall direction and the averages for every slab are computed for the quantities of interest: defining $B(y_{\text{bin}})$ as the value of the phase variable B in a bin centered at y_{bin} we have $B(y_{\text{bin}}, t) = \int dx \int_{y_{\text{bin}} - \Delta/2}^{y_{\text{bin}} + \Delta/2} dy B(\mathbf{r}, t) / \Delta$. This method is very easy to implement but the slab width has to be chosen carefully. If too wide, the resolution will be poor, while if too small, the statistics will be poor. We compute the streaming velocity in each bin as a running average during the simulation. This definition gives good results, as can be seen for the system in Fig. 2.

Following the kinetic definition of temperature³²

$$T(y_{\text{bin}}, t) = \frac{\sum_{i \in \text{bin}} m_i [\mathbf{v}_i(t) - \mathbf{u}(y, t)] [\mathbf{v}_i(t) - \mathbf{u}(y, t)]}{2N_{\text{bin}}(t)}, \quad (16)$$

the PUT has been devised such that each slab is associated with a friction coefficient, which accounts for density fluctuations across the channel.

The last system we consider is a homogeneous fluid evolving according to the SLLOD equations of motion to compare its Lyapunov spectra,

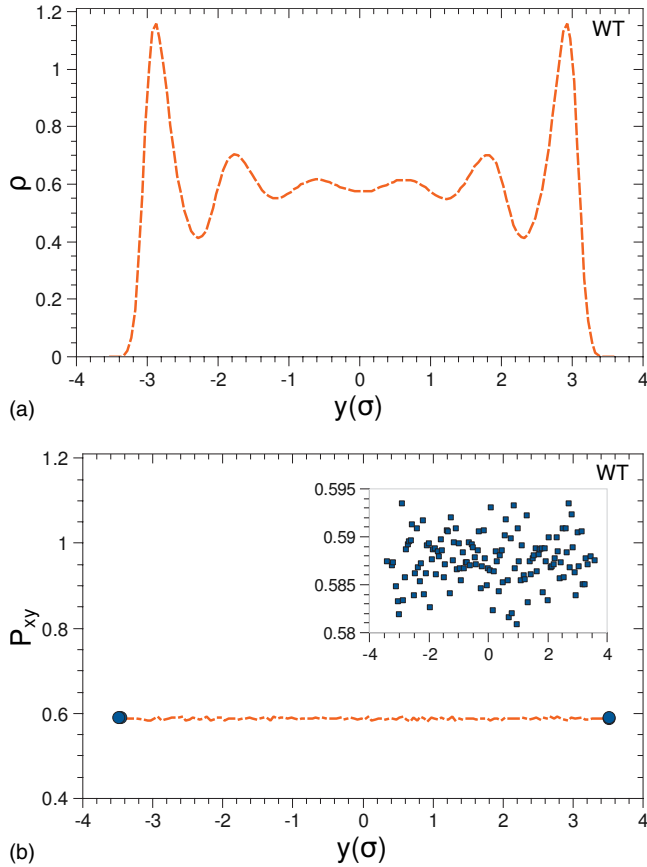


FIG. 2. WT system for Couette flow with applied shear rate $\dot{\gamma}=1.0$. (a) Cross section profile of density; (b) xy component of the pressure tensor P_{xy} (the blue circles indicate the pressure values at the wall), the plot inserted on the top right corner is a zoom of the pressure. The system consisted of 45 fluid particles at a density $\rho_f=0.6$ in a channel of width $L_y=6.82$ and 40 wall particles at a density $\rho_w=0.8$. Walls thermostated at $T=1.0$.

$$\dot{\mathbf{q}}_i = \mathbf{p}_i/m_i + \mathbf{i}\dot{\gamma}y_i, \quad (17)$$

$$\dot{\mathbf{p}}_i = \mathbf{F}_i - \mathbf{j}\dot{\gamma}p_{xi} - \xi\mathbf{p}_i. \quad (18)$$

Because the system is homogeneous, appropriate PBCs are required (the well known Lees–Edwards³³ PBCs), and the thermostat employed assumes a linear velocity profile, given that the relatively low strain rate employed is a reasonable choice.

For the computation of the pressure tensor we employ the method of planes technique.³⁴ Instead of dividing the channel into slabs, it is divided into planes equally spaced, and the velocity of the particles crossing the planes and the force between the particles on opposite sides of the planes are coupled to generate the potential and kinetic components of the pressure tensor, respectively,

$$P_{\alpha\gamma}^U(y) = \frac{1}{2A} \sum_{ij} F_{\alpha ij} [\Theta(y_i - y)\Theta(y - y_j) - \Theta(y_j - y)\Theta(y - y_i)], \quad (19)$$

$$P_{\alpha\gamma}^K(y) = \lim_{\tau \rightarrow \infty} \frac{1}{A\tau} \sum_{0 < t_{i,m} < \tau} \sum_i p_{\alpha i}(t_{i,m}) \text{sgn}[p_{\gamma i}(t_{i,m})], \quad (20)$$

where i and j are the particle indices, $\alpha=x$ or y , Θ is the Heaviside step function, and m indexes the times at which the particle crosses the plane. This method allows a high resolution, because unlike the bin method the separation of planes does not influence the statistical precision of the pressure tensor. The method of planes has been used exclusively for the computation of the pressure tensor as we do not need that level of precision for the determination of the other quantities we consider.

As a further check we computed the velocity and speed distribution to see if they followed the Maxwell–Boltzmann statistics. We considered only the x component (direction of the flow) for the velocity distribution. The two distribution functions are computed for each slab across the channel,

$$f(v_x, y_{\text{bin}}) = \sqrt{\frac{m(y_{\text{bin}})}{2\pi k_B T(y_{\text{bin}})}} \exp\left[-\frac{m(y_{\text{bin}})v_x^2(y_{\text{bin}})}{2k_B T(y_{\text{bin}})}\right], \quad (21)$$

$$f(v, y_{\text{bin}}) = \left(\frac{m(y_{\text{bin}})}{k_B T(y_{\text{bin}})}\right) v(y_{\text{bin}}) \exp\left[-\frac{m(y_{\text{bin}})v^2(y_{\text{bin}})}{2k_B T(y_{\text{bin}})}\right]. \quad (22)$$

We do not show the plots, however, because the results are in good agreement for all systems.

IV. LOCALIZATION OF LYAPUNOV EXPONENTS ACROSS THE CHANNEL

To understand if and how the dynamics is altered by the use of the thermostat, we compute the spectra of subsystem Lyapunov exponents (see Ref. 23) of the fluid and which part of the channel contributes the most to a particular exponent. It is important to underline that the spectra considered here do not involve all the degrees of freedom of the system (fluid, walls, and thermostat degrees of freedom). Following the same technique used in Ref. 23, we consider only the dynamics of the fluid phase space. In order to do this, we define displacement vectors $\delta\Gamma_{i \dots j}^l \equiv [\delta\Gamma_i^l, \dots, \delta\Gamma_j^l]$ where $\delta\Gamma_i^l = [\delta\mathbf{q}_i^l, \delta\mathbf{p}_i^l]$ gives the components of the l th displacement vector associated with the i th particle, and the displacement vectors associated with all other particles are set to zero. Therefore, we define the subsystem Lyapunov exponents as

$$\lambda_F^l = \lim_{t \rightarrow \infty} \lim_{\delta\Gamma_{i \dots j}^l \rightarrow 0} \frac{1}{t} \ln \left(\frac{|\delta\Gamma_{i \dots j}^l(t)|}{|\delta\Gamma_{i \dots j}^l(0)|} \right), \quad (23)$$

where the particle indices $i \dots j$ are for the fluid particles. Our technique differs from a previously attempted way to achieve such splitting which involved projecting the whole phase space onto the low dimensional Hamiltonian phase space.³⁵ We note that the fluid subsystem Lyapunov exponents approach the true Lyapunov exponents in the limit of zero coupling with the walls.

To compute the spectral density of the subsystem Lyapunov exponents inside the channel we use the Lyapunov vectors $\delta\Gamma^l$ associated with the exponents. These vectors indicate the direction in which expansion/compression in phase

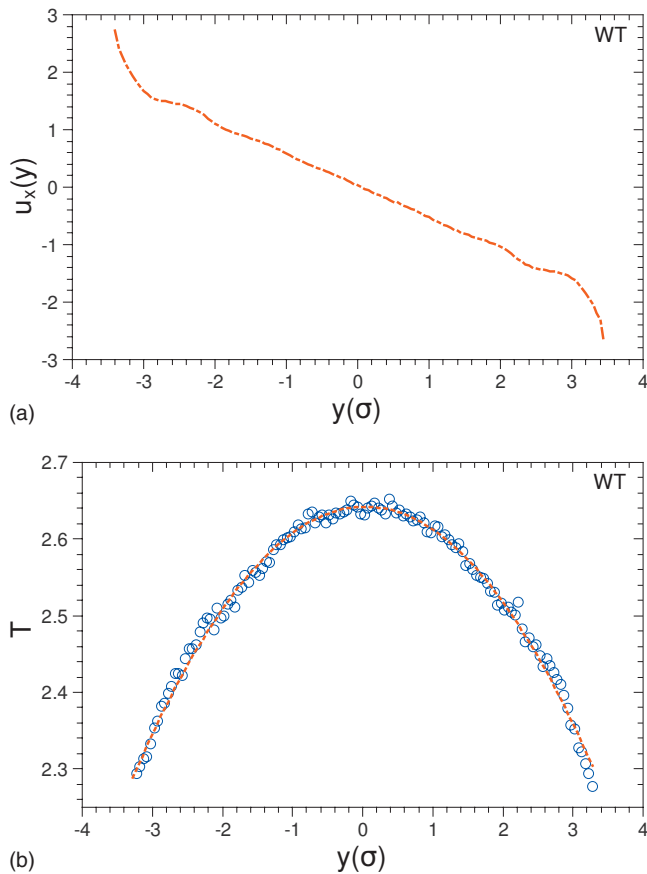


FIG. 3. WT system for Couette flow with applied shear rate $\dot{\gamma}=1.0$ as with Fig. 2. (a) Streaming velocity; (b) temperature (circle represents data points while the dashed line is a quadratic fit to the data).

space occurs for each Lyapunov exponent at an instant in time. If the vectors are orthonormalized we can introduce a squared norm³⁶

$$\gamma_i^j = (\delta \mathbf{q}_i^j)^2 + (\delta \mathbf{p}_i^j)^2, \quad (24)$$

such that

$$0 \leq \gamma_i^j \leq 1 \quad \text{and} \quad \sum_i \gamma_i^j = 1. \quad (25)$$

This quantity tells us how, for each exponent l , the contributions are distributed among the particles. After computing γ_i^j every selected number of time steps, we localize the particle i in the real space across the channel and, at this position, sum the contributions for each exponent. On average this will give us the exponent localization. We consider the localization only for the y direction using the same resolution of 0.05 as for the mechanical properties.

V. RESULTS

The results are organized such that for every thermostatting device, the plots relative to the profiles (for density, temperature, streaming velocity, and xy component of the pressure tensor across the channel) for vibrating and frozen walls are superimposed.

We start by examining the properties of the WT systems that, mimicking real experiments, will be our reference system (Figs. 2 and 3). The applied shear rate is set at the wall

to $\dot{\gamma}=1.0$. For a sliding boundary (SB) Couette flow this is a high value;^{3,37} however, to make possible a comparison between the Lyapunov spectra for the SB systems and the homogeneous system (SLLD), a high value of shear rate is necessary. We can observe that the mechanical properties show sensible profiles: the streaming velocity is linear in a region of 3σ in the middle of the channel with an effective strain rate of $\dot{\gamma}_{\text{eff}}=0.55$, the density shows packing close to the walls but the oscillations decrease rapidly away from the boundaries. The shear stress is constant inside the channel, with a value of $P_{xy} \approx 0.59$, and the temperature shows a quadratic profile, as predicted by the hydrodynamic equations,

$$\rho \frac{\partial u_x}{\partial t} = \rho F_e - \frac{\partial P_{xy}}{\partial y}, \quad (26)$$

$$\rho F_e = 0, \quad (27)$$

and because at steady state $\partial u_x / \partial t = 0$,

$$\frac{\partial P_{xy}}{\partial y} = 0 \Rightarrow P_{xy} = \text{const.} \quad (28)$$

For the temperature we have

$$\lambda \frac{d^2 T}{dy^2} = -\eta \left(\frac{\partial u_x(y)}{\partial y} \right)^2, \quad (29)$$

from which we obtain

$$T(y) = -\frac{\eta \dot{\gamma}^2}{2\lambda} y^2 + Cy + D, \quad (30)$$

with C and D being constants of integration, and λ is the thermal conductivity of the fluid. The average temperature of the fluid is $T=2.5$.

The speed and velocity distributions are in good agreement with the theoretical curves relative to the temperature inside each bin [i.e., Eqs. (21) and (22)]. In all the systems in which the thermostat is directly applied to the fluid, the temperature, for both wall and fluid, has been set by taking the average value of the temperature across the channel for the wall thermostated system. This is to ensure that when a comparison between the systems is attempted they are at an equivalent state point and to avoid temperature gradients at the wall-fluid interface. However, this is not a common practice. In fact, exactly what is the right average temperature of a fluid is something that cannot be known in advance from the knowledge of the boundary conditions. A trial simulation would be required, undoing the advantage of a simulation performed by thermostating the fluid. A set of simulations with wall and fluid temperature kept at $T=1.0$ has also been performed. The results show a higher disagreement even with respect to the system with the temperature set at $T=2.5$. Such disagreement can be summarized by a more accentuated packing close to the walls and layering across the channel, a quantitative difference in shear stress due to the lower kinetic component of the pressure tensor, and slightly shifted values of speed distributions toward smaller velocity values.

We now look at the PUT system (Figs. 4 and 5). The density for the vibrating wall system shows typical fluctua-

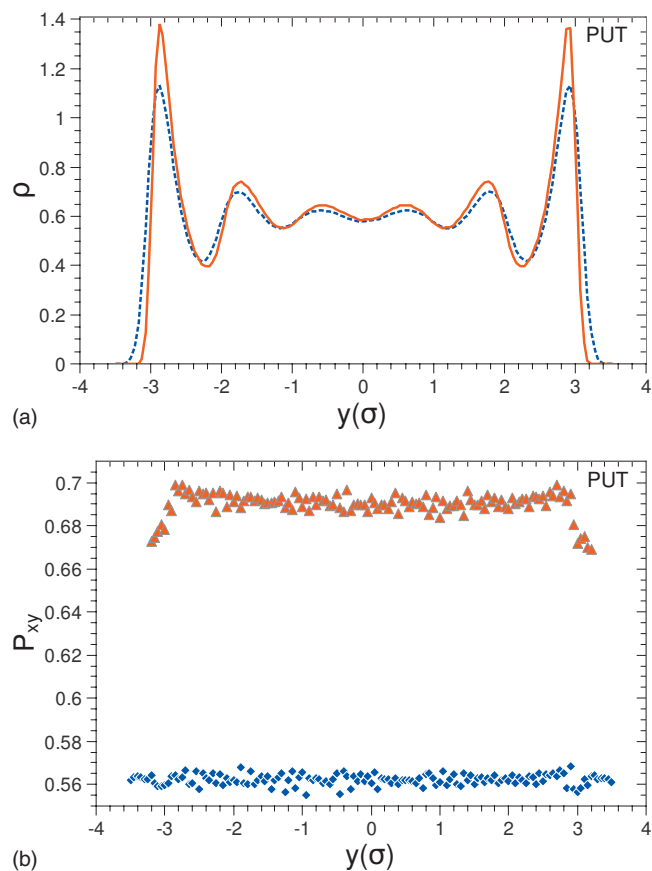


FIG. 4. PUT system for Couette flow with applied shear rate $\dot{\gamma}=1.0$. (a) Cross section profile of density; (b) xy component of the pressure tensor P_{xy} . The system consisted of 45 fluid particles at a density $\rho_f=0.6$ in a channel of width $L_y=6.82$ and 40 wall particles at a density $\rho_w=0.8$. Blue (dashed line and diamond symbols): fluid thermostated at $T=2.5$ and wall at $T=1.0$. Red (solid line and triangle symbols): fluid thermostated at $T=2.5$ and frozen walls.

tions; however, for the frozen wall system the peaks at the boundaries and in the middle of the pore are higher than for the vibrating wall system, indicating a more pronounced layering. This situation is also present in the PBT systems that are discussed later in this section. In the frozen wall system the channel is slightly narrower than for vibrating wall systems because the fluid pushes the vibrating wall particles away. In fact, apart from the harmonic potential, no other constraints have been used to keep the wall layers in place to avoid the introduction of spurious dynamics. The shear stress for the vibrating wall system is roughly correct in value but shows a slightly parabolic profile. This means that a pressure gradient is present across the fluid even if the system has reached a steady state. This is in contrast with the hydrodynamic predictions and means that the fluid shows unphysical properties. For rigid walls the parabolic profile is more strongly emphasized and furthermore the value shows a net increase, which is significantly different to that for the vibrating wall.

The streaming velocities are, for both vibrating and frozen walls, comparable with the wall thermostated system. However, the induced strain rate for frozen walls is slightly higher, $\dot{\gamma}\approx 0.62$, while for vibrating walls it is $\dot{\gamma}\approx 0.51$. This means that the slip for rigid walls is lower than for vibrating

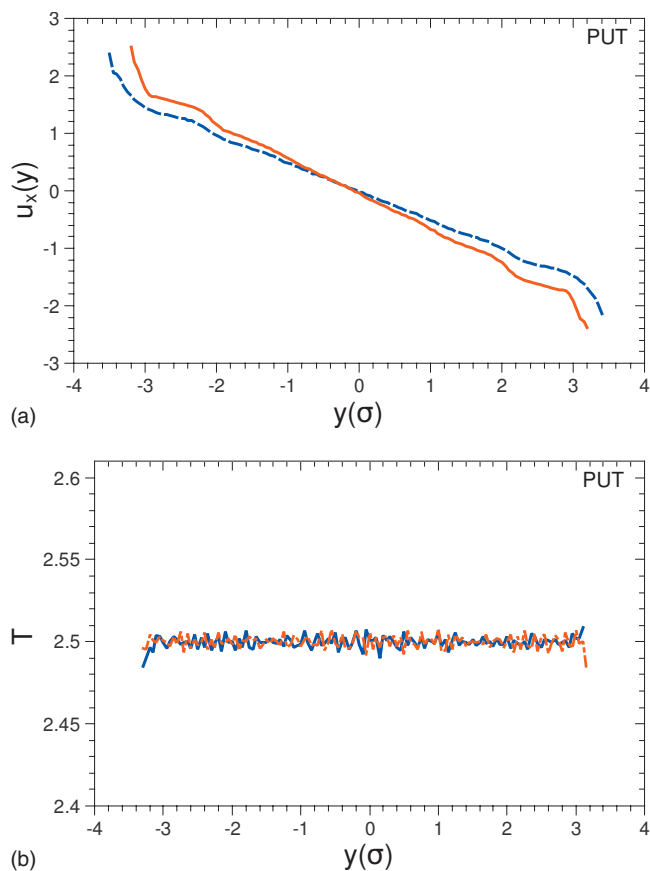


FIG. 5. PUT system for Couette flow with applied shear rate $\dot{\gamma}=1.0$ as with Fig. 4. (a) Streaming velocity; (b) temperature.

walls. This has been verified by performing a set of simulations in which only one wall was allowed to shear, keeping the opposite one stationary. The stationary wall was in turn allowed to vibrate or kept frozen. The slip, defined as the value of the linear interpolation of the streaming velocity at the intersection with the steady wall, has been computed for different values of wall density and strain rate (the strain rates were of the order of 10^{-2} to avoid temperature gradients across the channel and keep the velocity profile roughly linear even close to the wall). What we observed was a slip for the vibrating wall systems (slip ≈ 0.06), double the value for the rigid wall (slip ≈ 0.03). However, if the wall density exceeded a value of $\rho_w \approx 1.2$ (in two dimensions this implies a quasismooth surface) the trend was reversed. This can be explained by considering the geometry of the wall (Fig. 6). Let us consider for simplicity a hard sphere potential and a fluid particle coming toward the wall at a 45° angle with respect to the normal to the wall surface. When the wall is

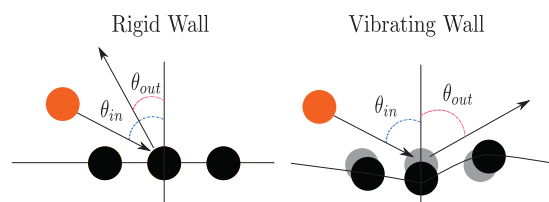


FIG. 6. Schematic representation of the effect that a frozen wall has on the slip with respect to a vibrating wall.

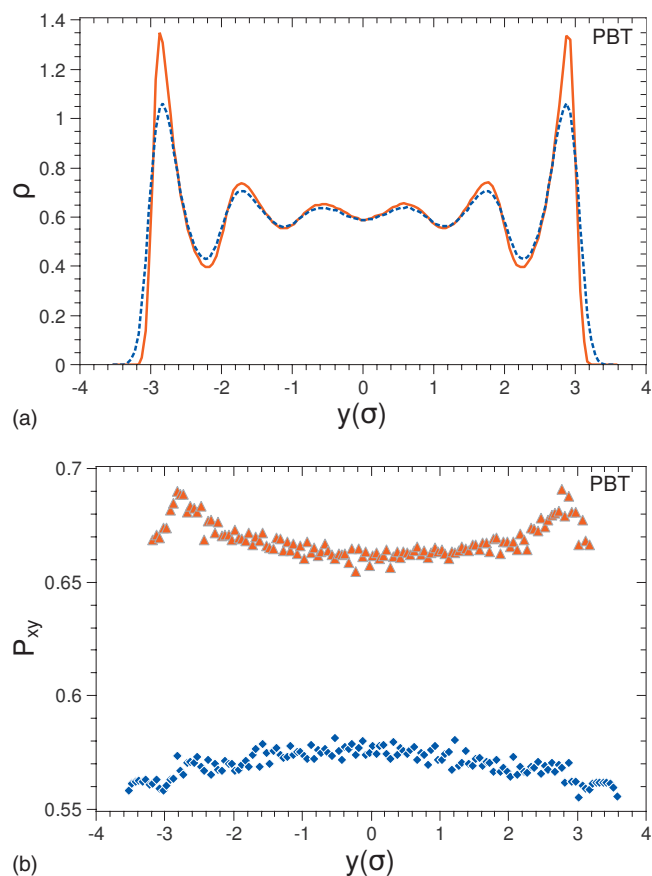


FIG. 7. PBT system (the thermostat does not account for density fluctuations) for Couette flow with applied shear rate $\dot{\gamma}=1.0$. (a) Cross section profile of density; (b) xy component of the pressure tensor P_{xy} . The system composition is the same as for Figs. 4 and 5. Blue (dashed line and diamond symbols): fluid thermostated at $T=2.5$ and wall at $T=1.0$. Red (solid line and triangle symbols): fluid thermostated at $T=2.5$ and frozen walls.

frozen it behaves like an array of hard scatterers and the chances for the fluid particle to be reflected back are high (this decreases the slip), while when the wall is able to vibrate, the wall particle will partly absorb the fluid momenta and, shifting backward, allows the fluid particle to keep moving toward the same direction thus increasing the slip. The temperature profile in the PUT system is constant across the channel as imposed by the thermostat.

For the PBT (Figs. 7 and 8), we impose a linear profile with a strain rate obtained by interpolation from the PUT instead of the WT system. This is to avoid imposing a profile that would be unnatural for a thermostated fluid. The density and streaming velocity profiles for either the vibrating or frozen walls are qualitatively and quantitatively the same as for the PUT. The shear stress, however, shows two opposite profiles, a concave parabolic profile for the vibrating wall system, while convex for the rigid wall system, and a significant difference between the two of ≈ 0.1 . The temperature for the vibrating wall system is roughly constant in the center of the channel but increases at the wall interface where there is a steep density increase and the velocity gradient differs from the assumed value. When the walls are frozen we observe an accentuated parabolic profile, higher temperature close to the walls and lower in the center of the channel. Such erratic and unphysical profiles can lead to wrong con-

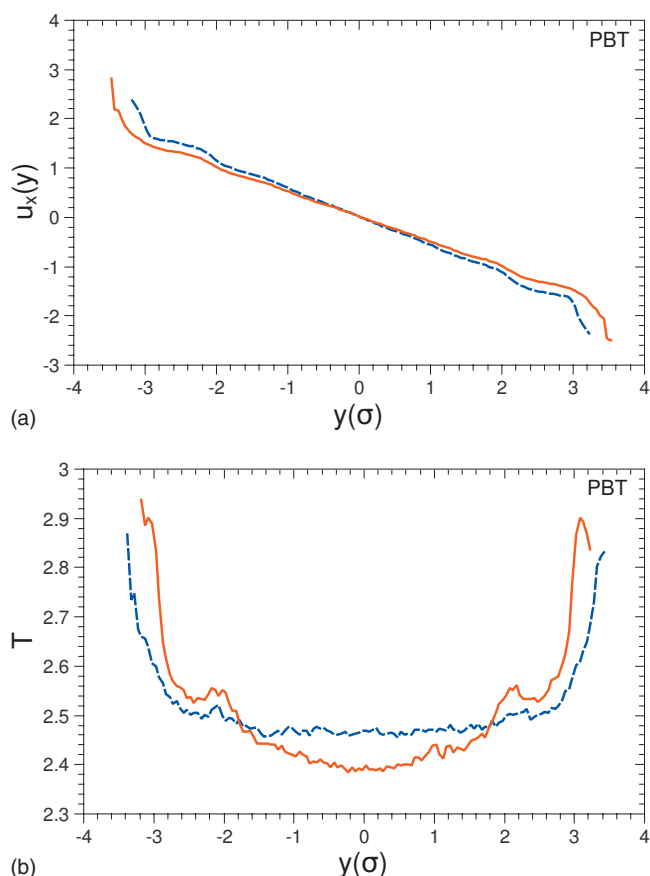


FIG. 8. PBT system (the thermostat does not account for density fluctuations) for Couette flow with applied shear rate $\dot{\gamma}=1.0$ as with Fig. 7. (a) Streaming velocity; (b) temperature.

clusions in studies where thermal properties are involved. Also evident are kinks in the temperature due to the steep density gradients that the homogeneous thermostat is not able to account for. For the PBT system with frozen walls we also checked if an independent control of the temperature in the x and y directions would improve the mechanical response due to the temperature anisotropy present in a strongly driven fluid. However, the mechanical properties did not show any significant difference.

The last system simulated was a PUT (Fig. 9) in which the temperature imposed across the channel was parabolic and obtained by quadratic interpolation from the wall thermostated system, i.e., the temperature in each bin is thermostated to the equivalent temperature in each corresponding bin in the WT system. As one would expect for the system with vibrating walls, the profiles are the same as for the WT system; however, for rigid walls the streaming velocity shows a higher velocity gradient and the pressure again displays the irregular and slightly parabolic profile.

We now analyze the effect of the thermostats on the subsystem Lyapunov spectra of the confined system and the Lyapunov spectrum of the homogeneous system. All the spectra plotted refer to the exponents for the phase space generated by the fluid particles only. We show four spectra, one for the WT system and one for a SLLOD system, at the same average state point as the WT (together in Fig. 10), and two for the PUT system in Fig. 11 (either vibrating or frozen

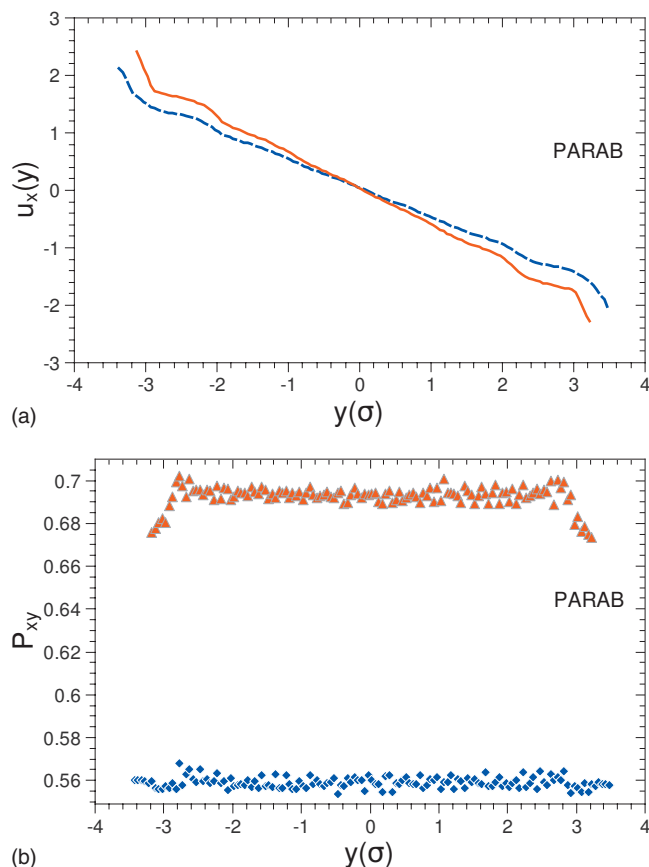


FIG. 9. Parabolic temperature profile thermostated system (the thermostat accounts for density fluctuations) for Couette flow with applied shear rate $\dot{\gamma}=1.0$. (a) Cross section profile of streaming velocity; (b) xy component of the pressure tensor P_{xy} . The system composition and state point are the same as for Figs. 4 and 5.

wall). The SLLOD spectrum has six characteristic exponents that we omit from Fig. 10 because they are related to conservation properties that do not exist for the confined fluid. Four exponents are related to the momentum and center of mass conservation in the x and y directions for the SLLOD algorithm, one exponent is related to kinetic energy conservation and has a value of zero, and the last one to the non-autonomous character of the dynamics.²⁰ The first five exponents are identically zero. In Fig. 10 we can see that, because the chaoticity of the fluid is determined mainly by the actual velocity gradient inside the fluid and its density and temperature, the spectra of the two systems look basically the same with comparable maximum Lyapunov exponents. The confinement does not seem to affect the spectra's shape (the meaning of which has not been completely understood yet³⁸), which is influenced for the most part by the overall fluid density that determines the collision rate. The only appreciable difference is in the sum of the exponents, which is 0 for the fluid subsystem exponents in the confined system and ≈ -0.2 for the homogeneous system. This is not surprising and is a natural consequence of the dissipative character of the SLLOD equations of motion^{18,20,39,40} [Eqs. (17) and (18)]. The phase space contraction for Eqs. (17) and (18) is strictly connected with the entropy production and heat dissipation by the relation

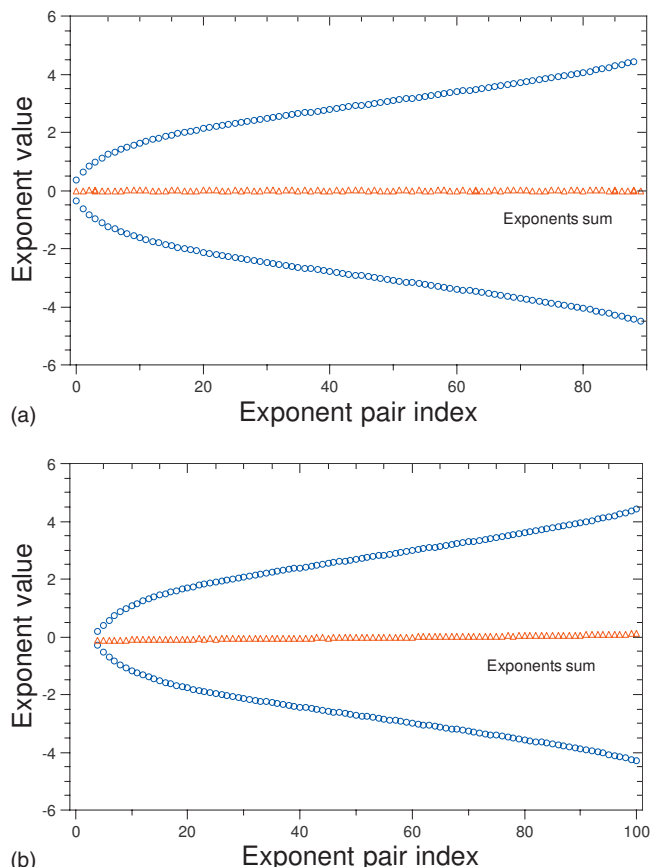


FIG. 10. (a) Fluid subsystem Lyapunov spectra for WT system, 45 fluid particles at a density $\rho_f=0.6$, 40 wall particles at a density $\rho_w=0.8$, channel width $y=6.82$, Couette flow with effective velocity gradient $\dot{\gamma}=0.55$, walls thermostated at $T=1.0$ (reduced units). (b) Lyapunov spectra for a SLLOD system, 50 fluid particles at a density $\rho_f=0.6$, velocity gradient $\dot{\gamma}=0.55$, temperature $T=2.5$.

$$\dot{S}/k_b = \langle \Lambda \rangle = - \sum_i \lambda_i = -g \langle \dot{\xi} \rangle > 0, \quad (31)$$

where g is the number of degrees of freedom thermostated, $\Lambda \equiv (\partial/\partial\Gamma) \cdot \dot{\Gamma}$ is the so-called phase-space compressibility factor, and $\langle \dot{\xi} \rangle$ is the averaged value over time of the ther-

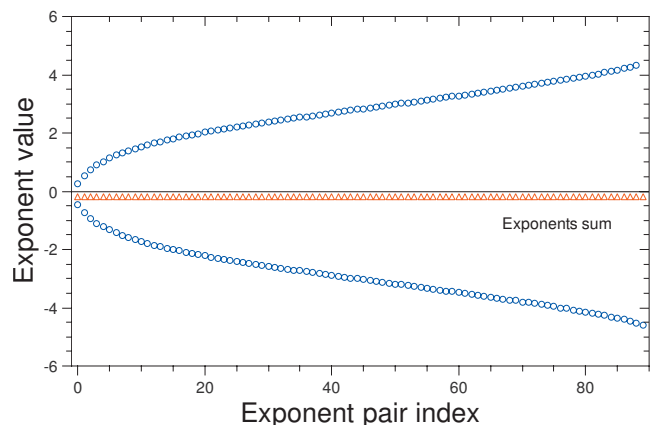


FIG. 11. Fluid subsystem Lyapunov spectrum for Couette flow with a PUT and vibrating walls. This spectrum is, within limits of error, indistinguishable for both PBT and PUT systems either with vibrating walls or frozen walls. The system composition and state point are the same as for Figs. 4 and 5.

mostat friction coefficient. The equations of motion of the fluid for the confined system, Eqs. (9) and (10), however, do not show explicitly the thermostat's friction coefficient, which is included only in the wall equations of motion. Note that if the Lyapunov spectrum of the confined system was calculated (i.e., the full spectrum which includes both the walls and fluid) rather than the fluid subsystem exponents, the sum of the exponents would also be expected to be negative (see Ref. 23). This is why the negative pair sum appears only in the Lyapunov spectra for the SLLOD system.

In Fig. 11, we display the fluid subsystem Lyapunov spectra for a PUT system with vibrating walls. Because the thermostat acts independently in every bin the number of friction coefficients is equal to the number of bins, so the above relation, Eq. (31), should account for a sum over the bins $\sum_i^{\text{bin}} \xi_i$. The PUT in Fig. 11, however, shows a higher dissipation than the equivalent SLLOD system. This could be due to the fact that to obtain the same velocity gradient, the walls have to perform more work on the fluid particles and thus even the heat absorbed by the thermostat is higher. This, according to Eq. (31), would result in a more negative pair sum. This spectrum is indistinguishable from the spectrum computed for a PUT system with frozen walls and the PBT system with either vibrating or frozen walls. The specific implementation of the wall does not seem to affect the exponents. Their value reflects the mixing of the fluid particles in the coordinate and velocity spaces. The mixing is determined mainly by temperature, number density, and velocity gradient; therefore, these quantities being equal, the spectra will look the same. Several wall implementations have been tested, including a repulsive potential wall, and the spectra did not show any appreciable difference.

The last results presented in Fig. 12 refer to the Lyapunov localization. The Lyapunov spectra characterize the system as a whole. However, because the system is inhomogeneous we want to examine where, inside the channel, the chaotic nature of the fluid receives its largest contributions. Using Eq. (25) we quantify these contributions, and we do this for the whole Lyapunov spectrum.

The largest Lyapunov exponents quantify the fastest dynamical events happening in the system (i.e., particle collisions). For large systems with conserved quantities (e.g., energy) and spatial symmetries (PBCs), the smallest Lyapunov exponents represent the particles' collective behaviors that manifest themselves with periodic structures present in the perturbations associated with the smallest exponents called Lyapunov modes.^{41–43} However, because our system is small, confined and thermostated, the small exponents do not organize themselves into modes, even if they can still be regarded as characterizing the system's global properties. Our interest is in the Lyapunov localization inside the channel and therefore we only consider the phase space generated by the fluid. This allows also to compare the Lyapunov localization for exponents characterized by the same dimensionality. Figure 12(a) shows the localization for the fluid subsystem exponents in the WT system, while Fig. 12(b) shows the localization for the PBT system with frozen walls. In Fig. 12(a) we purposely choose to exclude the phase space generated by the wall, while in Fig. 12(b) the wall particles,

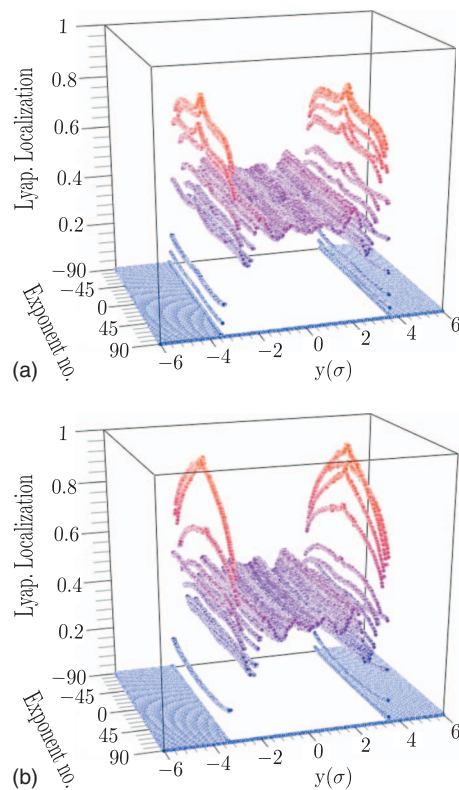


FIG. 12. (a) Fluid subsystem Lyapunov exponent localization for a Couette flow fluid thermostated through conduction to the walls. 40 fluid particles at a density $\rho_f=0.6$, strain rate $\dot{\gamma}=0.55$, wall thermostated at $T=1.0$ (reduced units). (b) Fluid subsystem Lyapunov exponent localization for a profile biased thermostated fluid (PBT) with frozen walls (from which comes no contribution).

not having any degrees of freedom, do not add dimensionality to the phase space. The localization exponents have been normalized with respect to the largest (of both systems, WT and PBT) exponent contribution. In this way, a quantitative comparison between the two systems is also possible. For both the WT and PBT systems the fluctuations across the channel show a strong correlation with the density; in fact, the more a particular area of the channel is populated, the more it is likely to contribute to chaos. This effect is simply due to the presence of more particles there. Consideration of the deviations of the localization from the density profile indicates that the maximal exponents have a reduced contribution in the region near the walls, and the contribution is fairly uniform elsewhere. Conversely, when considering the smallest exponents, the particles near the wall have a considerably enhanced contribution. In fact, as we approach the smallest exponents, the more the localization is enhanced near the walls. Comparing the WT and PBT systems shows both a quantitative and qualitative change: for the WT system the change in the contribution as we go from the maximum to the minimum exponent assumes the shape of “braces,” while for the PBT system a bell shape is observed with a significantly high contribution from the minimum exponents. This result shows that the presence of a thermostat in the fluid coupled with a rigid wall distorts the dynamics, especially near the walls.

VI. CONCLUSIONS

In this work we have shown results concerning the use of thermostating devices for a highly confined fluid. The purpose is to cast light on the effects that a thermostat mechanism can have when used directly on fluid particles instead of applying it on the channel's walls, as in mimicking real experiments, to allow the heat produced in the fluid by the external force field to dissipate through them. We have looked how a number of properties change, either from a mechanical point of view, showing what happens to the shear stress, streaming velocity, density and temperature across the channel, and from a dynamical point of view by comparing the Lyapunov spectra for the fluid phase space.

From the analysis of these systems we conclude that, independent of the type of thermostat device used, the mechanical properties show significant variations, and all together they are never comparable to the WT system, in which case the profiles show good agreement with hydrodynamic predictions. The values of shear stress and shear rate are significantly different, the density shows stronger fluctuations, and the velocity distribution functions are not always in agreement with the theoretical curve (if the temperature is not chosen carefully). Thermostating the fluid improperly also gives rise to a different dynamics as can be seen from the analysis of the Lyapunov localization, the greatest difference being for the smallest Lyapunov exponents and close to the walls. The main conclusion to be drawn from this study is that thermostating a confined fluid can lead to significant unpredictable and unphysical material properties and underlying dynamics. Thermostating a strongly driven confined fluid should always be done by the action of the walls, mimicking nature as close as possible. Furthermore, freezing the walls (hence, by necessity requiring one to thermostat the fluid) should also be avoided to remove such artificial material and dynamical properties. Our results therefore suggest caution in interpreting the results of recent NEMD studies on confined systems, such as flows inside carbon nanotubes, in which the carbon nanotube atoms are frozen and the fluid molecules are thermostated.

¹D. J. Evans, W. G. Hoover, B. H. Failor, B. Moran, and A. J. C. Ladd, *Phys. Rev. A* **28**, 1016 (1983).

²B. D. Todd and P. J. Davis, *Mol. Simul.* **33**, 189 (2007).

³S. Y. Liem, D. Brown, and J. H. R. Clarke, *Phys. Rev. A* **45**, 3706

(1992).

⁴D. J. Evans and G. P. Morriss, *Statistical Mechanics of Nonequilibrium Liquids* (Cambridge University Press, London, 1990).

⁵V. P. Sokhan, D. Nicholson, and N. Quirke, *J. Chem. Phys.* **117**, 8531 (2002).

⁶J. A. Thomas and A. J. H. McGaughey, *Nano Lett.* **8**, 2788 (2008).

⁷Y. Leng and P. T. Cummings, *Phys. Rev. Lett.* **94**, 026101 (2005).

⁸V. P. Sokhan, D. Nicholson, and N. Quirke, *J. Chem. Phys.* **115**, 3878 (2001).

⁹J. Casas-Vázquez and D. Jou, *Rep. Prog. Phys.* **66**, 1937 (2003).

¹⁰D. J. Evans, *J. Stat. Phys.* **57**, 745 (1989).

¹¹D. J. Evans and L. Rondoni, *J. Stat. Phys.* **109**, 895 (2002).

¹²S. R. de Groot and P. Mazur, *Non-Equilibrium Thermodynamics* (Dover, New York, 1984).

¹³D. J. Evans and G. P. Morriss, *Phys. Rev. Lett.* **56**, 2172 (1986).

¹⁴W. G. Hoover, *Phys. Rev. A* **31**, 1695 (1985).

¹⁵I. Shimada and T. Nagashima, *Prog. Theor. Phys.* **61**, 1605 (1979).

¹⁶H. A. Posch and W. G. Hoover, *Phys. Rev. A* **38**, 473 (1988).

¹⁷H. A. Posch and W. G. Hoover, *J. Phys.: Conf. Ser.* **31**, 9 (2006).

¹⁸F. Frascoli, D. J. Searles, and B. D. Todd, *Phys. Rev. E* **73**, 046206 (2006).

¹⁹D. J. Searles, D. J. Evans, and D. J. Isbister, *Chaos* **8**, 337 (1998).

²⁰S. Sarman, D. J. Evans, and G. P. Morriss, *Phys. Rev. A* **45**, 2233 (1992).

²¹G. P. Morriss, *Phys. Rev. A* **37**, 2118 (1988).

²²T. Taniguchi and G. P. Morriss, *Phys. Rev. E* **66**, 066203 (2002).

²³S. Bernardi, B. D. Todd, D. J. Searles, J. S. Hansen, and F. Frascoli, *J. Chem. Phys.* **132**, 244508 (2010).

²⁴W. G. Hoover, C. G. Hoover, and J. Petracic, *Phys. Rev. E* **78**, 046701 (2008).

²⁵W. G. Hoover and C. G. Hoover, *Phys. Rev. E* **79**, 046705 (2009).

²⁶G. Benettin, L. Galgani, A. Giorgilli, and J. M. Strelcyn, *Meccanica* **15**, 9 (1980).

²⁷G. Benettin, L. Galgani, A. Giorgilli, and J. M. Strelcyn, *Meccanica* **15**, 21 (1980).

²⁸J. D. Weeks, D. Chandler, and H. C. Andersen, *J. Chem. Phys.* **54**, 5237 (1971).

²⁹M. P. Allen and D. J. Tildesley, *Computer Simulation of Liquids* (Oxford University Press, Oxford, 1987).

³⁰K. P. Travis, B. D. Todd, and D. J. Evans, *Phys. Rev. E* **55**, 4288 (1997).

³¹J. J. Erpenbeck, *Phys. Rev. Lett.* **52**, 1333 (1984).

³²B. D. Todd and D. J. Evans, *Phys. Rev. E* **55**, 2800 (1997).

³³A. W. Lees and S. F. Edwards, *J. Phys. C* **5**, 1921 (1972).

³⁴B. D. Todd, D. J. Evans, and P. J. Davis, *Phys. Rev. E* **52**, 1627 (1995).

³⁵H. A. Posch and W. G. Hoover, *Physica D* **187**, 281 (2004).

³⁶T. Taniguchi and G. P. Morriss, *Phys. Rev. E* **73**, 036208 (2006).

³⁷J. P. Ryckaert, A. Bellemans, G. Ciccotti, and G. V. Paolini, *Phys. Rev. Lett.* **60**, 128 (1988).

³⁸H. A. Posch and W. G. Hoover, *Phys. Rev. A* **39**, 2175 (1989).

³⁹E. G. D. Cohen, *Physica A* **213**, 293 (1995).

⁴⁰G. P. Morriss, *Phys. Rev. E* **65**, 017201 (2002).

⁴¹L. Milanović, H. A. Posch, and W. G. Hoover, *Mol. Phys.* **95**, 281 (1998).

⁴²C. Forster and H. A. Posch, *New J. Phys.* **7**, 32 (2005).

⁴³J.-P. Eckmann, C. Forster, H. A. Posch, and E. Zabey, *J. Stat. Phys.* **118**, 813 (2005).